Interactive Visualization of Time-Varying Hyperspectral Plant Images for High-Throughput Phenotyping

Feiyu Zhu[1], Yu Pan[1], Tian Gao[1], Harkamal Walia[2], Hongfeng Yu[1]
[1] Department of Computer Science and Engineering
[2] Department of Agronomy and Horticulture
University of Nebraska-Lincoln, Lincoln, NE, USA

***Abstract*—Analysis of hyperspectral images is of great importance in many scientific disciplines. Obtaining the spectral and spatial information simultaneously from time-varying hyperspectral images is a challenging task due to their high dimensionality. In this paper, we design an interface that allows users to study hyperspectral images interactively and obtain spectral features and enhanced images at the same time. The image fusion results change dynamically with the regions of interest selected by users and convey both the spatial and spectral information. We show the usefulness of our approach using time-varying hyperspectral plant images. We compare our method with existing hyperspectral image analysis techniques. Our evaluation indicates that our interface can help users determine important bands, identify regions of interest, and generate image fusion results for time-varying hyperspectral plant images.**

***Index Terms*—Hyperspectral images, Time-varying, Interactive visualization, High-throughput phenotyping**

I. Introduction

With advances in digital imaging technology, hyperspectral cameras have become more affordable and ubiquitous, leading to an exponential growth of high-throughput imaging systems in recent years [7], [18], [26]. These systems can non-destructively capture the high-resolution spatial and spectral information of objects. The resulting hyperspectral images have significantly boosted researchers' capability to obtain detailed traits in applications in various scientific disciplines, such as physics, biology, and geoscience.

Hyperspectral images are conventionally modeled as a 3D data block, known as a *hyperspectral cube*. The x and y dimensions reserve the spatial information of imaged objects. The z (or λ) dimension contains the spectral information that acts as a fingerprint for an object in the x and y space. A hyperspectral cube is formed by stacking the images taken at a sequence of wavelengths with a fixed view.

Researchers have developed plenty of approaches to analyzing hyperspectral images. A commonly used strategy is to apply *image fusion* techniques [16], [17], [22], [23] to summarize all hyperspectral images into a fused image for feature identification. There are also studies of using machine learning techniques, such as support vector machine (SVM) and convolutional neural network (CNN), to classify different regions [2], [15]. As hyperspectral imaging has been applied for plants, plant scientists would like to capture the distribution of biomarkers (e.g., water and chlorophyll) in a leaf and identify the spectral ranges where these biomarkers have strong interactions [7]. Traditional techniques cannot fulfill these emerging hyperspectral imaging analysis requirements, due to a loss of intrinsic relationships between the spatial and spectral information in fused images.

Scientists demand new tools to analyze and visualize hyperspectral images in both the 2D spatial space and the 1D spectral space. However, as an important data type in practical applications, hyperspectral images have not received considerable attention in visualization research so far. Although hyperspectral images can be conceptually modeled as a cube, they are different from traditional volume data and impose unique challenges of interpreting them. In a hyperspectral cube, the spatial dimensions and the spectral dimension have different physical meanings. In a traditional volume, 3D objects can be identified by their spatial characteristics (e.g., gradient [13], curvature [14], size, and occlusion [28]). However, these measures do not have comparable meanings in the spectral space. Therefore, the existing volume visualization techniques cannot be directly applied to hyperspectral cubes. The main objectives of studying hyperspectral images can be summarized as follows:

- Explore and identify bands with a strong spectral response.
- Calculate and explore spectral features for each pixel in the given bands.

The first objective focuses on reducing redundant information without compromising the original hyperspectral images. The second objective focuses on finding the most useful features that can well represent the hyperspectral images.

In our work, we develop an interactive visualization tool for hyperspectral images. Our new solution can facilitate users from different domains to interactively explore and discover features in regions of interest that may be difficult to identify using traditional techniques. Our major contributions are:

- A data model to describe a hyperspectral cube with uneven illumination.
- An information metric based design that allows users to find the important bands interactively.
- A new visualization design that enables users to gain

spatial and spectral information simultaneously from a hyperspectral cube.

We have demonstrated the effectiveness of our approach with time-varying hyperspectral datasets of plants which are collected using the high-throughput phenotyping system located at the Nebraska Innovation Campus.

II. Related Work

We review the existing analysis and visualization techniques for hyperspectral images.

A. Clustering-based Methods

Some clustering-based methods focus on finding the best bands [27], while others focus on comparing the spectral curves. Here, we mainly discuss the methods that compare the curves, as bands can be selected interactively in our design by users. As the substances are characterized by different spectral curves over all the bands, an intuitive solution is to cluster the spectral curves of all pixels into different groups according to their spectral curve shapes [20]. Clustering-based methods do not deal with the spectral features directly. They mainly compare each spectral curve with the cluster center and try to group these spectral curves. The methods that focus on find groups can partly achieve the second objective as the spectral features of the clustering centers can be easily found.

However, in practice, it is nearly impossible to maintain a homogeneous illumination during imaging, which leads to different intensities for the same substance. Therefore, the spectral curve of the same substance may have different scales in different positions. The substances cannot be correctly classified due to the effects of uneven illumination. We will illustrate this issue using a synthetic dataset in Section III.

B. Machine Learning-based Methods

Machine learning has been widely used for the classification of pixels in hyperspectral images. The supervised or non-supervised learning of spectra is developed to classify the regions in a 2D image based on certain properties. The maximum likelihood classification is commonly applied to remotely sensed optical data. The maximum likelihood calculates the probability that a pixel belongs to a cluster [15]. SVM with different kernels and CNN have also been used to reach a high accuracy of classification [2]. Although these methods work very well in some cases, the machine learning-based methods usually require a training process where labeled data or ground truth is needed. It becomes hard to apply these methods if a hyperspectral dataset contains no labels. There are studies of using unsupervised machine learning such as Self-Organizing Map (SOM) [25] to cluster hyper-dimensional data without labels. The results can be better than the k-means clustering for some hyperspectral images. Machine learning-based methods are similar to clustering based methods in terms of find spectral features. They partly achieve the second objective as the spectral features of the classified data can be found.

C. Image Fusion based Methods

Scientists also often leverage image fusion based methods to reduce a hyperspectral cube to a 2D image and try to maximize the information shown in the 2D image [16], [23]. Some dimension reduction methods (e.g., principal component analysis (PCA), discrete wavelet transform (DWT)) [17], [23] are commonly used for image fusion. For other image fusion techniques, usually, one or more cost functions are constructed and minimized to get 2D image fusion results [1].

Although PCA-based methods work very well at differentiating different pixels, they still have some disadvantages [10]. PCA treats all the bands as independent dimensions without considering the order of different bands. The result from PCA is dependent on the relative size of substances. The same substance may have different colors as the relative area of the object containing the substance may change [3], [5]. Statistics, such as skewness and kurtosis, have been used for the projection of hyperspectral data [8].

However, the traditional image fusion process suffers from certain problems. It can be hard to distinguish different substances from an image fusion result, and scientists need to retrieve the missing information by studying the entire images of different substances again. If there are many substances in the hyperspectral images, it is time-consuming for scientists to plot all the spectra and compare them pairwise. We will detail this issue in Section III.

D. Visualization based Techniques

To our knowledge, thus far, hyperspectral images have received relatively little attention in the area of visualization. Cui et al. [4] developed a visualization tool for image fusion using convex optimization. Kim et al. [12] developed an interactive visualization tool for hyperspectral images of historical documents based on image fusion. Kim et al. [11] used hyperspectral imaging to develop a 3D scanning system to enhance the quantification of reflectance of the surface of an object. Some work attempted to generate an enhanced fused image ready to be visualized on a display [21], but did not directly deal with the visualization of hyperspectral images.

III. Background

We revisit the background of hyperspectral imaging and discuss the advantages and the limitations of existing methods.

A. Hyperspectral Imaging

Different from VIS cameras, hyperspectral cameras can capture hundreds or thousands of images at a series of bands with a fixed view. The images can be stacked together to form a volume or a hyperspectral cube. As shown in Figure 2, the x and y dimensions of this cube provide the spatial information for each pixel in the image of objects. The λ dimension contains the spectral characteristics (or named *spectral curve*) for each pixel. Researchers have developed plenty of approaches to analyzing hyperspectral images. A commonly used strategy is to apply *image fusion* techniques [16], [17], [22], [23] to summarize all hyperspectral images into a fused image for studying objects, as shown in Figure 1 (b).

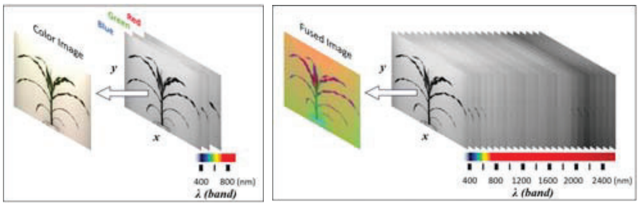

(a) (b)

Fig. 1: Comparison between plant images taken by (a) a VIS camera and (b) a hyperspectral camera.

B. Hyperspectral Cube

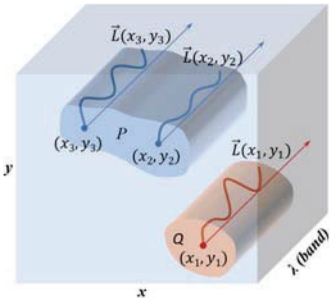

Fig. 2: The data model of hyperspectral cubes.

A set of hyperspectral images taken from the same scene can be stacked along the λ dimension to form a hyperspectral cube. For one hyperspectral image, a position (x, y) in the image corresponds to a pixel. As a hyperspectral cube is a stack of images, a position (x, y) corresponds to a set of voxels. The intensity values of this set of voxels form a spectral curve that reveals the spectral response of one point on an object in the real world. We denote the set of voxels for a position (x, y) as $\vec{L}(x, y)$. We define each object as a continuous area with only one type of substance. In practice, one object may reveal different spectral curves due to inhomogeneous illumination. For example, in Figure 2, we assume that the object P is subject to uneven illumination. Therefore, the spectral curve $\vec{L}(x_3, y_3)$ at the position (x_3, y_3) of P has stronger spectral response compared with the spectral curve $\vec{L}(x_2, y_2)$ at the position (x_2, y_2) of P. The shape of $\vec{L}(x_2, y_2)$ and $\vec{L}(x_3, y_3)$ are similar but the scales of them are different. For the position (x_1, y_1) on another object Q, the shape of the spectral curve $\vec{L}(x_1, y_1)$ is distinct from $\vec{L}(x_2, y_2)$ or $\vec{L}(x_3, y_3)$, which means that $\vec{L}(x_1, y_1)$ is from a different object.

C. Challenges of Hyperspectral Analysis

We use a synthetic dataset to illustrate the challenges of hyperspectral analysis. As shown in Figure 3 (a), we assume there are three substances, S_1, S_2, and S_3, in the dataset, colored as red, green, and blue, respectively. Figure 3 (d) shows their spectral curves with different shapes. We assume that there are 100 bands, leading to 100 images in total.

It is a challenge to distinguish these substances just using a few individual bands due to the similarities and differences of their hyperspectral curves. According to our model of hyperspectral cubes, we note that the study of it is equivalent to study the characteristics of the spectral curve $\vec{L}(x, y)$ of object S. An important fact in the hyperspectral data model is that whether the objects can be detected depends on the bands selected. This implication can be illustrated with the synthetic dataset in Figure 3. The substances S_1 and S_2 can be distinguished if all the bands are selected. However, if the bands ranging from 90 to 100 are selected, where the spectra for both substances are identical as shown in Figure 3 (d), these two substances S_1 and S_2 cannot be distinguished. When analyzing hyperspectral images of the plants, scientists may distinguish a plant from the background using just one image. However, the selected bands may not reveal the subtle details between the stem and leaves. Thus, in order to identify these substances, scientists usually need to explore the entire bands one by one and back and forth, which is cumbersome.

Moreover, hyperspectral images typically suffer from variation of illumination [9], [24]. We will demonstrate this phenomenon using the synthetic dataset. A pixel along the λ axis can be treated as one hyper-pixel in a high dimensional space. To illustrate the distribution of hyper-pixels, we select sample values from three bands at 15, 50, and 85. The hyper-pixels are then plotted in a 3D space using the sampled values. In an ideal case, where the illumination is even, the hyper-pixels for the three substances S_1, S_2, and S_3 in the synthetic dataset will appear as just three points in the high-dimensional space, as shown in Figure 3 (g).

However, in practice, there is usually uneven illumination, which leads to the scale changes of the hyperspectral curves. For example, Figure 3 (b) shows a simple example where the illumination is gradually reduced from the center, and Figure 3 (e) shows the corresponding scale changes of the hyperspectral curves compared to Figure 3 (a). In this case, the hyper-pixels of the three substances with uneven illumination form three rays in the high-dimensional space (Figure 3 (h)) instead of three points in the ideal case.

In practice, there may also be some blur caused by light interference or diffraction, as shown in Figure 3 (c). Figure 3 (f) shows the scale changes of the hyperspectral curves. In this case, the hyper-pixels can form into a set of rays of different substances in the high-dimensional space, as shown in Figure 3 (i).

We can express this phenomenon in the following equation for each spectral curve $\vec{L}(x, y)$:

$$\vec{L}(x, y, k, b) = k(x, y)\vec{L}(x, y) + b(x, y) \tag{1}$$

which means that a linear transform is applied on the spectral curve $\vec{L}(x, y)$, where $k(x, y)$ is the scale and $b(x, y)$ is a constant at a position (x, y).

Let $\vec{L}$ denote the whole hyperspectral cube, and K and B denote the scales and constants for all the positions. Then we have

$$\vec{L} = K\vec{L} + B \tag{2}$$

Due to interference among the light from different substances, images are usually blurred such that the intensity of one substance can change gradually to the intensity of another substance. This phenomenon can be expressed in the following equation:

$$\vec{L}(\sigma, \mu) = G(\sigma, \mu) * \vec{L}(k) = G(\sigma, \mu) * (K\vec{L} + B) \quad (3)$$

where $G(\sigma, \mu)$ is a Gaussian distribution with variance σ and mean μ, and $*$ means convolution operation. Based on our data model, normalization of hyperspectral curves can be a suitable way to reduce the effects of uneven illumination. The normalization is performed as dividing each spectral curve by the maximum value of that curve. We will show the effects of normalization in the next section.

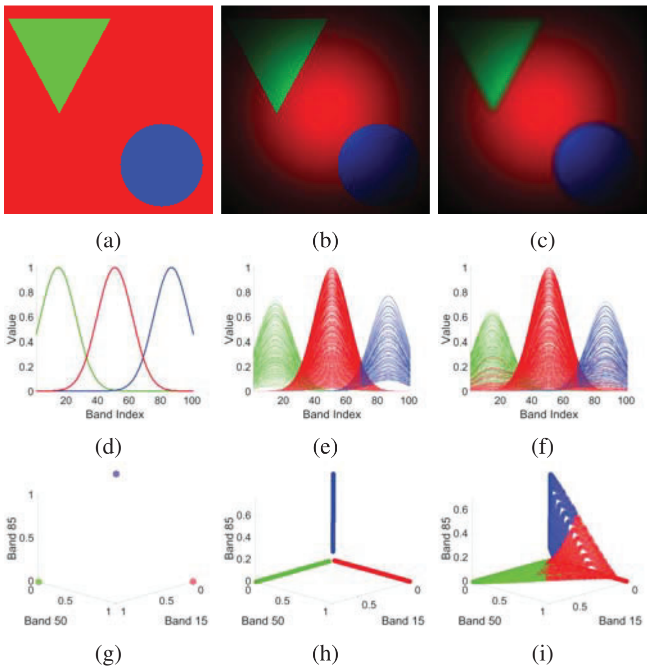

Fig. 3: The top row shows a simple synthetic dataset with three substances S_1, S_2, and S_3 with (a) even illumination, (b) uneven illumination, and (c) further Gaussian blur. The middle row shows the corresponding hyperspectral curves of the three substances under different illumination conditions. The bottom row shows the distribution of hyper-pixels of the three substances in a 3D space under each illumination condition. In each plot, red, green and blue correspond to S_1, S_2, and S_3, respectively.

D. Interactive Hyperspectral Visualization

A hyperspectral cube is fused into an image for visualization in conventional approaches. Every spectral curve is reduced to one pixel in the fused image. To process spectral curves, a metric that gives similar scores for spectra with similar shapes is desired. Generally, the spectral curves may be evaluated by their peaks, valleys, or curvature characteristics. An evaluation of all the spectral curves in a hyperspectral cube produces a score image that has the same dimension as all the hyperspectral images.

Since an object in a hyperspectral cube may not be known as *a priori* and whether it could be discovered strongly depends on the selection of bands, interactive selections of bands and regions of interest (ROI) are desired functions to study hyperspectral cubes. Real-time interaction is necessary for scientists to explore and learn features in both the spatial and spectral domains. The traditional methods typically generate a fused image where the image is considered optimal and cannot be changed once the image fusion is finished. Interactive tools can solve this problem intrinsically, as the information contained in the data cube can be dynamically extracted based on selections of users. Another advantage of the interactive exploration of the hyperspectral cube is that the spatial and spectral information are evaluated simultaneously. If the spatial ROIs are changed in the hyperspectral cube, the corresponding visualization results will also change.

IV. Rationale

We are inspired to develop an interactive tool to extract information inside hyperspectral cubes. We combine the spatial and spectral information to guide users in the exploration process. We summarize how we can make use of the global statistics and spectral features to design an interface to explore hyperspectral cubes. We will first use global statistics to help users select the important bands. Then, we will calculate the spectral features and allow users to select the spectral features. Finally, we will visualize the images based on user selections. The designed interface can not only achieve the two main objectives of studying hyperspectral images but also help users obtain good visualization results of the hyperspectral images.

A. Global Information

Generally, the dimension of hyperspectral images can be reduced by band selection [27]. In order to guide the user in the selection, we want to extract some global information. To get the global information of hyperspectral images, some metric is needed to evaluate each image. After consulting with domain experts, we noticed that the bands that they are interested in usually correspond to images with good contrast. An image with good contrast usually contains more information than images with low contrast. Entropy, as the most commonly used measure of the information of images, can be a useful metric for identifying images with good contrast. By assuming each pixel in an image is independent, we can obtain the probability of an intensity value in an image from the intensity histogram of the image.

Entropy has a tolerance for noise and other extrinsic imaging conditions. For example, if the intensity changes due to illumination while the distribution remains the same, the entropy remains the same. Noise or shift in pixels will only give small changes in entropy.

The substances can either absorb or emit light, and thereby the most important bands can correspond to either high or low-intensity values. However, entropy always has a large positive value when there is a good contrast in intensity, no matter if the intensity is at a peak or a valley. As users usually tend to select the peaks in a curve [19], the entropy curve can be very useful in helping users in selecting the important bands.

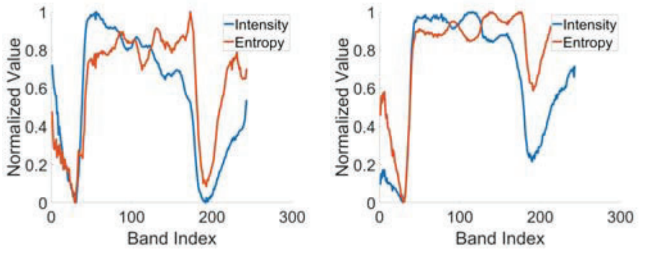

(a) (b)

Fig. 4: The average intensity and entropy plots for images across the entire bands. Two sets of hyperspectral images, including (a) maize and (b) sorghum, are used to show the generalization of the correlation between image intensity and entropy.

Some examples of the entropy and intensity over different bands are shown in Figure 4 for different datasets, which shows a high correlation between entropy and the average intensity of all sets of images. We will take advantage of this correlation to guide a user to select important bands for analysis.

The first objective, namely identifying important bands, can be achieved using a plot showing entropy of images over the band index. Once we select a band, the next objective is identifying the ROIs or substances in the given band by evaluating spectral curves. In the following section, the metrics used for evaluating spectral curves are introduced.

B. Spectrum Evaluation

An ideal classification of a 3D hyperspectral cube means the same substances in the 3D cube are grouped together, and the total number of clusters is equal to the total number of distinct substances. To classify all the substances in a cube, one way is to compare them like that in conventional clustering (e.g., k-means), and another way is to find a metric to characterize the spectral curves L. In our design, we use the second way for classification of spectral curves.

These metrics evaluate each spectral curve individually and have a lower complexity $O(N)$ that is preferable for real-time applications. As the calculation of a metric for one spectral curve is independent of the calculation for another, it is easy to parallelize the whole process of computation. We use GPU to accelerate the calculation and reach real-time user interaction.

The second objective of studying a hyperspectral cube is equivalent to find the scores of the spectral curves using some metrics. We visualize the results in a scatterplot and allow users to select the possible clusters of points interactively.

To evaluate spectral curves, many statistical metrics can be used. These metrics can be divided into three groups. The first group contains metrics that are related to the raw moment, such as intensity, energy, and Root Mean Square (RMS). The second group includes metrics that are related to the central moment, such as Mean Absolute Error (MAE), variance, standard deviation, skewness, and kurtosis. The third group contains metrics that are not directly related to the moment, such as minimum, maximum, range, percentile, entropy, and uniformity. Note that these metrics can be applied not only on the spectral curves directly but also on the nth derivative of the spectral curves. In our experiment, we also calculate the skewness and kurtosis of the first derivative and second derivative of the spectral curves. These derived features can be used to characterize the spectral curves in a non-linear way. However, as the number of features is still large, we want to reduce the number of redundant features used. In order to do that, we explored the relationship among these most commonly used features using the correlation analysis. Based on our correlation analysis, four features, intensity, skewness, kurtosis, and kurtosis of the first derivative, are kept for further analysis.

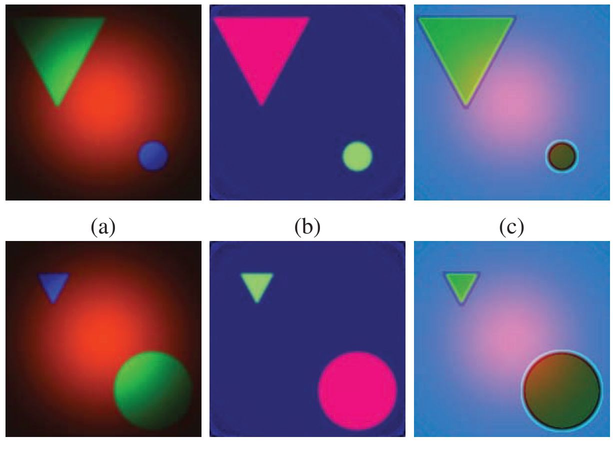

(a) (b) (c)

(d) (e) (f)

Fig. 5: The top row shows (a) the image fusion result generated using PCA, (b) the image fusion result generated using PCA after normalization of hyperspectral data, and (c) a fused image generated using three spectral features, intensity, skewness, and skewness of the first derivative. Each result in the bottom row is generated using the corresponding method in the top row for another synthetic dataset with the same substances but different object sizes.

Spectral feature analysis has advantages over PCA. Evaluation of features depends only on the characteristics of the spectral curve itself and does not depend on the comparison with other spectral curves. If pseudo-colors are used, the colors will be invariant with respect to the ROI selected, whereas the colors of the image generated by PCA vary for different ROIs of the same substances. PCA can project high dimensional data into low dimensions. However, the projected values only reveal the distances between different points without direct correspondence to the properties of the spectral curves. Different from PCA, in our method, the distribution of spectral features corresponds to different shapes of spectral curves. Some features, such as skewness, is scale-invariant, which means that spectral curves that are only different in scale will have the same feature value. This property can solve the problem caused by uneven illumination.

An example is shown in Figure 5, where two sets of syn-

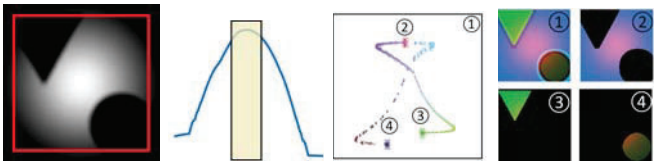

(a) (b) (c) (d)

Fig. 6: Examples of user selection. (a) A ROI in the red box of an image selected by the user. (b) Entropy plot where the bands can be interactively selected. (c) A 2D scatterplot formed using skewness and skewness of the first derivative. (d) Different regions of different selections in (c).

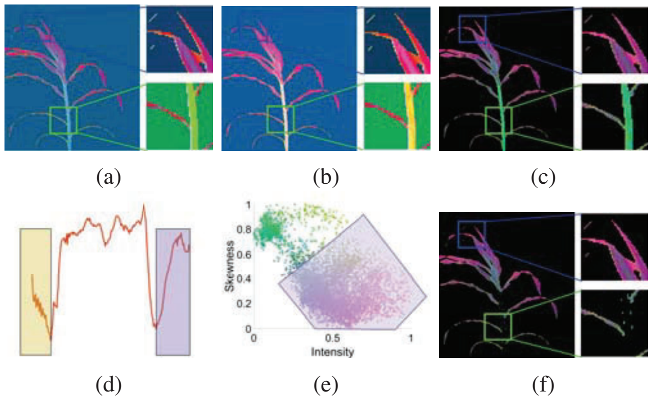

Fig. 7: Examples of user selection. (a) Image fusion based on PCA (b) Image fusion based on PCA after normalization. (c) Image fusion based on spectral features. (d) Selection of multiple bands as guided by the entropy curve. (e) A 2D scatterplot formed using intensity sum and skewness. (f) The leaves of the maize plant corresponding to the selection in (e).

thetic data with different object sizes are used. For example, the triangles in these two datasets have the same spectral shape, but different sizes. Figure 5 (a)(b)(c) are results for the first dataset, and Figure 5 (d)(e)(f) are results for the second dataset. Figure 5 (a)(d) are the image fusion results obtained by mapping the projected results corresponding to the largest three eigenvalues to the three channels in the RGB color space. These images are affected by the uneven illumination, and the colors of the same substance are different in these images. Figure 5 (b)(e) are obtained using the same method, but the input images are normalized by the intensity of the spectral curves. It can be seen that although normalization reduces the effects of uneven illumination, the results of PCA are still ROI-variant, as the colors of the triangles and circles are different in different images. Figure 5 (c)(f) is obtained by mapping intensity, skewness, and kurtosis to the three channels in RGB color space. We can see that the feature-based image fusion can not only reduce the effects of uneven illumination but also be ROI-invariant as the triangles and circles have consistent colors even if the sizes of the objects change. The feature-based image fusion can also enhance the boundaries more clearly, while it is hard to find the boundaries in the images obtained by PCA.

V. Interface Design

We have designed our interface to allow users to select and extract the features from the hyperspectral images easily. The whole image is usually selected in the traditional ways. However, analysis of the whole image may shadow some details that appear locally in a small region. To overcome this problem, we think it is necessary for users to define ROI based on their needs, where they are allowed to select a small region of the image for analysis. Figure 6 (a) shows an example of an ROI defined by the user. An entropy curve is calculated for all the images inside the selected ROI. Then, the user can continue to select the bands by examing the shape of the entropy curve, as shown in Figure 6 (b). The features of the corresponding spectral curves in the hyperspectral cube can be evaluated after the selection of bands. The yellow region in Figure 6 (b) shows a selection of bands. In Figure 6 (c), we give an example of the scatterplot of skewness and skewness of the first derivative. The user can use any combination of the four features we have kept after correlation analysis, which includes intensity sum, skewness, kurtosis, and skewness of the first derivative. Besides the scatterplot, other visual representations such as parallel coordinates may also be used to visualize multidimensional data [6]. We use scatterplots as they are already good enough for users to differentiate different substances in the hyperspectral images.

To visualize the scatterplot, we map each axis to one of the RGB channels. This kind of mapping allows users to find the correspondence between the points in the scatterplot and the objects in the fused image. The scatterplot can show a series of potential clusters, which can guide users to select the corresponding points for one particular substance or object. The user can brush the points in the plot, and a selection of points corresponds to a set of pixels in hyperspectral images. In the synthetic dataset, there are three substances S_1, S_2, and S_3. In Figure 6 (c), the pixels that correspond to them are enclosed by the red, green, and blue boxes, respectively. We visualize the selected pixels, as shown in Figure 6 (d), where regions of S_1, S_2, and S_3 are visualized using feature-based image fusion. There are four fused images in Figure 6 (d). Image 1 is the fused image where all the points are selected. Images 2, 3, and 4 are fused images that correspond to the selection of the points in the red, green, and blue boxes in Figure 6 (c), respectively.

VI. Results

A. Feature Selection

In this section, we show how our design can be used to explore and identify different substances in hyperspectral images interactively. We show the effectiveness of our design using datasets from plant science.

The hyperspectral images of plants were taken with 243 bands (wavelengths from 550 nm to 1700 nm). Then, the plants are placed in front of a white background in a chamber with illumination from the ceiling. The light causes uneven illumination where the upper part of the image has higher intensities. The hyperspectral bands can be divided into three ranges. The first range (550 nm - 700 nm) shows the response of photosynthetic pigments, such as chlorophyll. The second range (700 nm - 1100 nm) shows responses of cellular structures of plants. The third range (700 nm - 1750 nm) shows the absorption of water content in the plants. In our experiment, we will use only the first and the third ranges as phenotypes of plants in these ranges are well studied. In order to analyze the spectral features, the plants have to be segmented from the background. As the background is a whiteboard and has high reflectivity, we can segment the plant by removing pixels that have high intensities in the hyperspectral images.

A set of fused images based on PCA are shown in Figure 7 (a). The large image is the whole image, while the zoomed-in images are from two regions of the whole image as indicate by the green and blue boxes in the whole image. It can be seen that the colors in the whole image and the zoomed-in images are quite different, although they are from exactly the same dataset. As the relative size of the plant is different in the whole and zoomed-in images, the results generated by PCA are different. This kind of color variation caused by PCA will make it very hard to compare different ROIs in one dataset during user exploration. Another set of fused images based on PCA after normalization is shown in Figure 7 (b), where the whole image and the zoomed-in images also have different colors. Figure 7 (c) contains images generated using our interface. The whole image and the zoomed-in images have exactly the same colors, which makes it quite convenient for scientists to study different ROIs freely and compare different parts of the plant.

Figure 7 (f) shows the selection of bands where the bands in two ranges are selected in this case. Figure 7 (e) is the scatterplot of intensity and skewness. The red points correspond to the plant leaves while the green points correspond to the stem. Here we show an example of selecting the plant leaves. As shown in the fused image in Figure 7 (f), the leaves of the maize plant can be easily segmented for the whole image as well as the zoomed-in images by selecting the same region in the scatterplot in Figure 7 (e). As our interface is based on spectral features, it is ROI-invariant. This kind of user selection is hard to realize using previous methods as they rely on the comparison between different spectral curves and are not stable with respect to selections of different ROIs.

B. Time-Varying Selection

The time-varying hyperspectral images are the hyperspectral images of plants taken over some time. As the shapes and structures of plants change when they grow, analysis of time-varying hyperspectral images is difficult using traditional methods. As our method is based on spectral features, it can be used not only to compare different ROIs but also to compare plants at different time points. We give an example of a set of time-varying hyperspectral images of a maize plant taken over 25 days. We first find the corresponding scatterplots similar as the one shown in Figure 7 (e) for all 25 days. Then, we stack these 25 scatterplots to form a 3D scatterplot, as shown in Figure 8 (a). The points belong to different parts of the plant can be easily selected. For example, a selection as shown in the top view of the 3D scatterplot in Figure 8 (a) corresponds to the stem of the plant. Note that the selection here corresponds to the results from 25 days. Selected images from 5 selected days (with a 5-day interval) are shown in Figure 8 (b). The remaining leaves of these 5 days are shown in Figure 8 (d). With our interface, the user can view the changes in different parts of the plant over time with just one selection. For example, it can be easily observed that the length of the stem and the number of leaves change over time. We have tested our design for several datasets, including sorghum, maize, and tomato. Previous methods cannot provide such an easy kind of selection for the analysis of time-varying hyperspectral images as they are not ROI-invariant. If the first two axes of PCA results are used to form scatterplots and plots from 25 days are stacked together, as the sizes of the plants change over time, a selection in the stacked scatterplots can not lead to a clean selection of either stems or leaves.

VII. Conclusion

In this work, we propose a series of techniques for exploring time-varying hyperspectral images. Since the hyperspectral cube formed by hyperspectral images has one spectral dimension, the traditional image fusion methods lose information by fusing all the images. We define the data model for hyperspectral images and propose a new design that utilizes global information and spectral features. In the traditional image fusion methods, each image is treated as an individual dimension without considering the relationship between images. The novelty of our work is the combination of global information and spectral features in the design of the interface. The global statistics such as entropy is utilized to measure the global features, while some metrics such as intensity and skewness are used to measure spectral features. The global features can help users identify the most important bands as users tend to select bands with high entropy. After the selection of bands, we exploit 3D scatterplots of spectral features that allow users to select the feature points. After the selection of points, the corresponding substances in the time-varying hyperspectral images will be visualized. Our design can lead to clear separation of different substances for plants, which are difficult to achieve using current methods. We show that our design is invariant to the selection of ROIs, and it provides an easy comparison between different regions or different sets of hyperspectral images at different times. In future work, we will try to combine the hyperspectral images with other types of images, such as RGB and fluorescent images.

VIII. Acknowledgment

This research has been sponsored by the National Science Foundation through grants DBI-1564621, OIA-1736192, and IIS-1423487. The authors would like to acknowledge the staff members at the University of Nebraska-Lincoln's Greenhouse Innovation Center for their assistance in data collection.

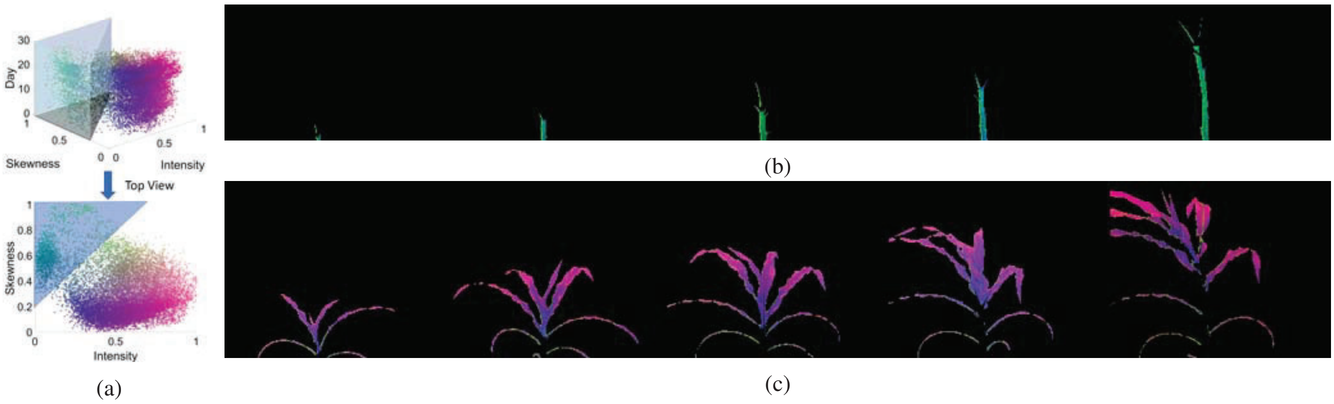

Fig. 8: Examples of user selection for a time-varying dataset. (a) 3D scatterplot of the spectral features of one maize plant over 25 days. The selection of the leaf points is performed on the top view of this scatterplot. (b) The selected stems from day 1, 6, 11, 16, and 21. (c) The remaining leaves from these five days.

References

[1] J. M. Bioucas-Dias, A. Plaza, G. Camps-Valls, P. Scheunders, N. Nasrabadi, and J. Chanussot. Hyperspectral remote sensing data analysis and future challenges. *IEEE Geoscience and Remote Sensing Magazine*, 1(2):6–36, 2013.

[2] Y. Chen, H. Jiang, C. Li, X. Jia, and P. Ghamisi. Deep feature extraction and classification of hyperspectral images based on convolutional neural networks. *IEEE Transactions on Geoscience and Remote Sensing*, 54(10):6232–6251, 2016.

[3] S.-S. Chiang, C.-I. Chang, and I. W. Ginsberg. Unsupervised target detection in hyperspectral images using projection pursuit. *IEEE Transactions on Geoscience and Remote Sensing*, 39(7):1380–1391, 2001.

[4] M. Cui, A. Razdan, J. Hu, and P. Wonka. Interactive hyperspectral image visualization using convex optimization. *IEEE Transactions on Geoscience and Remote Sensing*, 47(6):1673–1684, 2009.

[5] R. P. Desale and S. V. Verma. Study and analysis of pca, dct & dwt based image fusion techniques. In *Signal Processing Image Processing & Pattern Recognition (ICSIPR), 2013 International Conference on*, pages 66–69. IEEE, 2013.

[6] N. Elmqvist, P. Dragicevic, and J.-D. Fekete. Rolling the dice: Multidimensional visual exploration using scatterplot matrix navigation. *IEEE Transactions on Visualization and Computer Graphics*, 14(6):1539–1148, 2008.

[7] N. Fahlgren, M. A. Gehan, and I. Baxter. Lights, camera, action: high-throughput plant phenotyping is ready for a close-up. *Current Opinion in Plant Biology*, 24:93–99, 2015.

[8] X. Geng, L. Ji, and K. Sun. Principal skewness analysis: algorithm and its application for multispectral/hyperspectral images indexing. *IEEE Geoscience and Remote Sensing Letters*, 11(10):1821–1825, 2014.

[9] G. Healey and D. Slater. Models and methods for automated material identification in hyperspectral imagery acquired under unknown illumination and atmospheric conditions. *IEEE Transactions on Geoscience and Remote Sensing*, 37(6):2706–2717, 1999.

[10] N. P. Jacobson and M. R. Gupta. Design goals and solutions for display of hyperspectral images. *IEEE Transactions on Geoscience and Remote Sensing*, 43(11):2684–2692, 2005.

[11] M. H. Kim, T. A. Harvey, D. S. Kittle, H. Rushmeier, J. Dorsey, R. O. Prum, and D. J. Brady. 3D imaging spectroscopy for measuring hyperspectral patterns on solid objects. *ACM Transactions on Graphics (TOG)*, 31(4):38, 2012.

[12] S. J. Kim, S. Zhuo, F. Deng, C.-W. Fu, and M. Brown. Interactive visualization of hyperspectral images of historical documents. *IEEE Transactions on Visualization and Computer Graphics*, 16(6):1441–1448, 2010.

[13] G. Kindlmann and J. W. Durkin. Semi-automatic generation of transfer functions for direct volume rendering. In *Proceedings of The 1998 IEEE Symposium on Volume Visualization*, pages 79–86. ACM, 1998.

[14] G. Kindlmann, R. Whitaker, T. Tasdizen, and T. Moller. Curvature-based transfer functions for direct volume rendering: Methods and applications. In *Visualization, 2003. VIS 2003. IEEE*, pages 513–520. IEEE, 2003.

[15] S. Kuching. The performance of maximum likelihood, spectral angle mapper, neural network and decision tree classifiers in hyperspectral image analysis. *Journal of Computer Science*, 3(6):419–423, 2007.

[16] S. Li, X. Kang, and J. Hu. Image fusion with guided filtering. *IEEE Transactions on Image Processing*, 22(7):2864–2875, 2013.

[17] S. Li, B. Yang, and J. Hu. Performance comparison of different multi-resolution transforms for image fusion. *Information Fusion*, 12(2):74–84, 2011.

[18] G. Lu and B. Fei. Medical hyperspectral imaging: a review. *Journal of Biomedical Ooptics*, 19(1):010901, 2014.

[19] R. Maciejewski, Y. Jang, I. Woo, H. Jänicke, K. P. Gaither, and D. S. Ebert. Abstracting attribute space for transfer function exploration and design. *IEEE Transactions on Visualization and Computer Graphics*, 19(1):94–107, 2013.

[20] D. Manolakis, D. Marden, and G. A. Shaw. Hyperspectral image processing for automatic target detection applications. *Lincoln Laboratory Journal*, 14(1):79–116, 2003.

[21] A. Meka and S. Chaudhuri. A technique for simultaneous visualization and segmentation of hyperspectral data. *IEEE Transactions on Geoscience and Remote Sensing*, 53(4):1707–1717, 2015.

[22] G. Piella. Image fusion for enhanced visualization: A variational approach. *International Journal of Computer Vision*, 83(1):1–11, 2009.

[23] D. K. Sahu and M. Parsai. Different image fusion techniques–a critical review. *International Journal of Modern Engineering Research (IJMER)*, 2(5):4298–4301, 2012.

[24] T. W. Sawyer, A. S. Luthman, and S. E. Bohndiek. Evaluation of illumination system uniformity for wide-field biomedical hyperspectral imaging. *Journal of Optics*, 19(4):045301, 2017.

[25] K. Tasdemir and E. Merényi. Exploiting data topology in visualization and clustering of self-organizing maps. *IEEE Transactions on Neural Networks*, 20(4):549–562, 2009.

[26] C. Toth and G. Jóźków. Remote sensing platforms and sensors: A survey. *ISPRS Journal of Photogrammetry and Remote Sensing*, 115:22–36, 2016.

[27] Q. Wang, F. Zhang, and X. Li. Optimal clustering framework for hyperspectral band selection. *IEEE Transactions on Geoscience and Remote Sensing*, 56(10):5910–5922, 2018.

[28] L. Yu and H. Yu. Boundary-structure-aware transfer functions for volume classification. In *SIGGRAPH Asia 2017 Symposium on Visualization*, page 10. ACM, 2017.